NONLINEAR DIFFUSION

Erkut Erdem[*]

Hacettepe University

March 9th, 2013

CONTENTS

1 PERONA-MALIK TYPE NONLINEAR DIFFUSION

The main theory behind nonlinear diffusion models is to use nonlinear PDEs to create a scale space representation that consists of gradually simplified images where some image features such as edges are maintained or even enhanced. The earliest nonlinear diffusion model proposed in image processing is the so-called *anisotropic diffusion*[1] by Perona and Malik [4].

In their formulation, they replaced the constant diffusion coefficient of linear equation by a smooth nonincreasing diffusivity function g with $g(0) = 1$, $g(s) \geq 0$, and $\lim_{s\to\infty} g(s) = 0$. As a consequence, the diffusivities become variable in both space and time. The Perona-Malik equation is

$$\frac{\partial u}{\partial t} = \nabla \cdot (g(|\nabla u|)\nabla u) \tag{1}$$

with homogeneous Neumann boundary conditions and the initial condition $u^0(x) = f(x)$, f denoting the input image.

Perona and Malik suggested two different choices for the diffusivity function:

$$g(s) = \frac{1}{1 + s^2/\lambda^2}\,, \tag{2}$$

$$g(s) = e^{-\frac{s^2}{\lambda^2}} \tag{3}$$

[*]erkut@cs.hacettepe.edu.tr

[1]In fact, Perona-Malik equation is an isotropic nonhomogeneous equation as it uses a scalar-valued diffusivity. A true example of anisotropic diffusion model, edge-enhancing diffusion [6], will be summarized in Section 3.

where λ corresponds to a contrast parameter. These functions share similar characteristics, and result in similar effects on the diffusivities.

We review the 1D physical analysis of the Perona-Malik diffusion below since it clearly demonstrates the role of the contrast parameter λ and the main behavior of the equation [7]. For 1D case, the Perona-Malik equation is as follows:

$$\frac{\partial u}{\partial t} = \frac{\partial}{\partial x} \underbrace{\left(g(|u_x|)u_x\right)}_{\Phi(u_x)} = \Phi'(u_x)u_{xx} \tag{4}$$

with $g(|u_x|) = \frac{1}{1+|u_x|^2/\lambda^2}$ or $g(|u_x|) = e^{-\frac{|u_x|^2}{\lambda^2}}$.

Figure 1 shows the diffusivity functions and the corresponding flux functions for linear diffusion and Perona-Malik type nonlinear diffusion. One can easily observe that for linear diffusion the diffusivity is constant ($g(s) = 1$), which results in a linearly increasing flux function. As a result, all points, including the discontinuities, are smoothed equally. For Perona-Malik, the diffusivity is variable and decreases as $|u_x|$ increases. It is evident that the decay in diffusivity is particularly rapid after the contrast parameter λ. This leads to two different behaviors in the diffusion process. Since $\frac{\partial u}{\partial t} = \Phi'(u_x)u_{xx}$, for the points where $|u_x| < \lambda$, $\Phi'(u_x) > 0$ which corresponds to lost in the material. For the points where $|u_x| > \lambda$, on the contrary, $\Phi'(u_x) < 0$ which generates an enhancement in the material. Hence, although the diffusivity is always nonnegative, one can observe both *forward* and *backward* diffusions during the smoothing process, and the contrast parameter λ separates the regions of forward diffusion from the regions of backward diffusion.

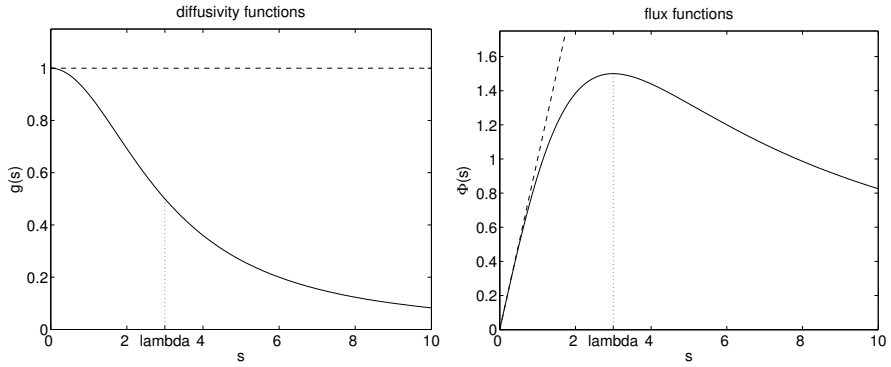

Figure 1: Diffusivities and the corresponding flux functions for linear diffusion (*plotted in dashed line*) and Perona-Malik type nonlinear diffusion (*plotted in solid line*). For Perona-Malik diffusivity $g(s) = \frac{1}{1+s^2/\lambda^2}$ is used with $\lambda = 3$.

If we consider the 2D case, the diffusivities are reduced at the image locations where $|\nabla u|^2$ is large. As $|\nabla u|^2$ can be interpreted as a measure of edge likelihood, this means that the amount of smoothing is low along image edges. In particular, the contrast parameter λ specifies a measure that determines which edge points are to be preserved or blurred during the diffusion process. Even edges can be sharpened due to the local backward diffusion behavior as discussed for the 1D case. Since the backward diffusion is a well-known ill-posed process, this may cause an instability, the so-called

(a) (b) (c)

Figure 2: The staircasing effect. (a) Original noisy image. (b) Perona-Malik diffusion. (c) Regularized Perona-Malik diffusion.

staircasing effect, where a piece-wise smooth region in the original image evolves into many unintuitive piecewise constant regions. Figure 2 shows an example where this instability occurs. The unintuitive regions such as the one at the woman's face and shoulder are clearly visible in Figure 2(b). A possible solution to this drawback is to use regularized gradients in diffusivity computations [2] (Figure 2(c)).

Replacing the diffusivities $g(|\nabla u|)$ with the regularized ones $g(|\nabla u_\sigma|)$ leads to the following equation:

$$\frac{\partial u}{\partial t} = \nabla \cdot (g(|\nabla u_\sigma|)\nabla u) \tag{5}$$

where $u_\sigma = G_\sigma * u$ represents a Gaussian-smoothed version of the image. Taking the equivalence of the Gaussian smoothing and the linear scale space into account, ∇u_σ can also be considered as the gradient computed at a specific scale $\sigma > 0$.

Some example results of regularized Perona-Malik filtering with different diffusion times are shown in Figure3 and Figure 4. It is evident from these images that the corresponding smoothing process diminishes noise while retaining or even enhancing edges since it considers a kind of a priori edge knowledge.

Numerical Implementation

For numerical implementation, we use central differences to approximate the gradient magnitude at a pixel (i, j) in the diffusivity estimation, $g_{i,j} = g(|\nabla u_{i,j}|)$:

$$|\nabla u_{i,j}| = \sqrt{\left(\frac{du_{i,j}}{dx}\right)^2 + \left(\frac{du_{i,j}}{dy}\right)^2} \approx \sqrt{\left(\frac{u_{i+1,j} - u_{i-1,j}}{2}\right)^2 + \left(\frac{u_{i,j+1} - u_{i,j-1}}{2}\right)^2}. \tag{6}$$

The Perona-Malik equation (Equation 1) is first discretized w.r.t. spatial variables.

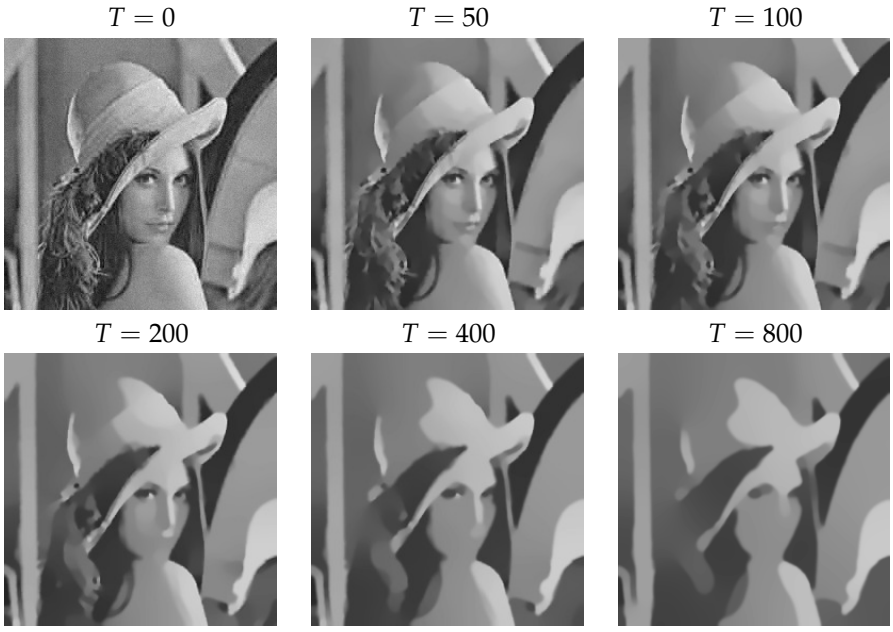

Figure 3: Reg. Perona-Malik results for different diffusion time ($\lambda = 1$, $\sigma = 1$).

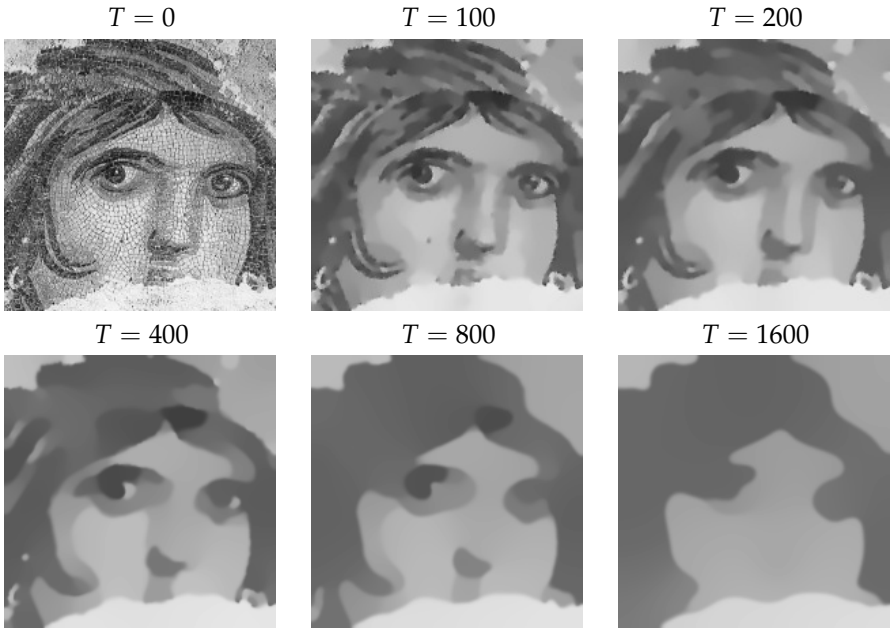

Figure 4: Reg. Perona-Malik results for different diffusion times ($\lambda = 1$, $\sigma = 1$).

This results in the following space-discrete equation:

$$\begin{aligned} \frac{\partial u}{\partial t} &= \frac{\partial}{\partial x}\left(g(|\nabla u|)u_x\right) + \frac{\partial}{\partial y}\left(g(|\nabla u|)u_y\right), \\ \frac{du_{i,j}}{dt} &= g_{i+\frac{1}{2},j}\cdot\left(u_{i+1,j}-u_{i,j}\right) - g_{i-\frac{1}{2},j}\cdot\left(u_{i,j}-u_{i-1,j}\right) \\ &+ g_{i,j+\frac{1}{2}}\cdot\left(u_{i,j+1}-u_{i,j}\right) - g_{i,j-\frac{1}{2}}\cdot\left(u_{i,j}-u_{i,j-1}\right). \end{aligned} \tag{7}$$

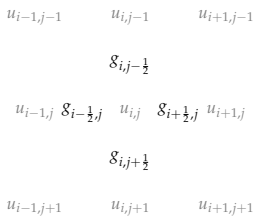

Figure 5: Discretization grid used in (Equation 7).

This discretization scheme requires the diffusivities to be estimated at mid-pixel points (Figure 5). They are simply computed by taking averages of the diffusivities over neighboring pixels:

$$g_{i\pm\frac{1}{2},j} = \frac{g_{i\pm1,j} + g_{i,j}}{2}, \qquad g_{i,j\pm\frac{1}{2}} = \frac{g_{i,j\pm1} + g_{i,j}}{2}\ . \tag{8}$$

The time derivative in (Equation 7) can be discretized using forward difference. This yields an iterative scheme with an explicit time discretization, where homogeneous Neumann boundary condition is imposed along the image boundary

$$\begin{aligned} \frac{u_{i,j}^{k+1} - u_{i,j}^{k}}{\Delta t} &= g_{i+\frac{1}{2},j}^{k} \cdot u_{i+1,j}^{k} + g_{i-\frac{1}{2},j}^{k} \cdot u_{i-1,j}^{k} + g_{i,j+\frac{1}{2}}^{k} \cdot u_{i,j+1}^{k} + g_{i,j-\frac{1}{2}}^{k} \cdot u_{i,j-1}^{k} \\ &- \left(g_{i+\frac{1}{2},j}^{k} + g_{i-\frac{1}{2},j}^{k} + g_{i,j+\frac{1}{2}}^{k} + g_{i,j-\frac{1}{2}}^{k}\right) \cdot u_{i,j}^{k} \end{aligned} \tag{9}$$

with Δt denoting the time step. For the Perona-Malik diffusion, the stability requirement is again $\Delta t \leq 0.25$.

2 Total Variation (TV) Regularization

Rudin et al. [5] formulated image restoration as minimization of the total variation (TV) of a given image under certain assumptions on the noise. The Total Variation (TV) regularization model is generally defined as:

$$E_{TV}(u) = \int_{\Omega} \left(\frac{1}{2}(u-f)^2 + \alpha|\nabla u|\right) dx \tag{10}$$

where

- $\Omega \subset \mathbb{R}^2$ is connected, bounded, open subset representing the image domain,
- f is an image defined on Ω,
- u is the restored version of g,

- $\alpha > 0$ is a scalar.

The gradient descent equation for Equation (10) is defined by

$$\frac{\partial u}{\partial t} = \nabla \cdot \left(\frac{\nabla u}{|\nabla u|} \right) - \frac{1}{\alpha}(u - f); \quad \left. \frac{\partial u}{\partial n} \right|_{\partial\Omega} = 0 \,. \tag{11}$$

Since the value of α specifies the relative importance of the fidelity term, it can be interpreted as a scale parameter that determines the level of smoothing. In Figure 6, the role of this parameter is illustrated. The restored images are given in Figure 6(b)-(d). As it can be clearly seen, level of smoothing increases with increasing α.

In the original formulation of Rudin et al., the observed image f was assumed to be degraded by additive Gaussian noise with zero mean and known variance σ^2. Hence, in order to restore a given image, they propose to solve the constrained optimization problem

$$\min_u \int_\Omega |\nabla u| dx \tag{12}$$

subject to

$$\int_\Omega (u - f)^2 dx = \sigma^2 \,. \tag{13}$$

When TV regularization is defined as a constrained optimization problem, $\frac{1}{\alpha}$ can be considered as a Lagrange multiplier, which has to be determined by taking the given constraint into account.

TV regularization can be associated with a nonlinear diffusion filter, the so-called *TV flow* [1, 3]. Ignoring the fidelity term in Equation (11) leads to the PDE

$$\frac{\partial u}{\partial t} = \nabla \cdot (g(|\nabla u|)\nabla u) \tag{14}$$

with $u^0 = f$ and the diffusivity function $g(|\nabla u|) = \frac{1}{|\nabla u|}$. Notice that this diffusivity function has no additional contrast parameter as compared with the Perona-Malik diffusivities. Figure 7 and Figure 8 depict TV scale space examples sampled at different diffusion times for two different images. It is evident from these images that the corresponding smoothing process yields segmentation-like, piecewise constant images.

Numerical Implementation

The evolution equation of u (11) can be discretized by using standard finite differences. An important point is that the solution of TV regularization or equivalently TV flow leads to singular diffusivities as shown in Equation (14). In numerical implementations based on standard discretization, this leads to stability problems as the image gradient tends to zero. A common solution to this problem is to add a small positive constant ϵ to image gradients.

After ϵ-regularization, the space-discrete version of Equation (11) can be written as:

$$
\begin{aligned}
\frac{\partial u}{\partial t} &= \frac{\partial}{\partial x}\left(\frac{u_x}{\sqrt{|\nabla u|^2+\epsilon^2}}\right)+\frac{\partial}{\partial y}\left(\frac{u_y}{\sqrt{|\nabla u|^2+\epsilon^2}}\right)-\frac{1}{\alpha}(u-f) \\
&= \frac{u_{xx}\left(u_y^2+\epsilon^2\right)-2u_xu_yu_{xy}+u_{yy}\left(u_x^2+\epsilon^2\right)}{\left(u_x^2+u_y^2+\epsilon^2\right)^{\frac{3}{2}}}-\frac{1}{\alpha}(u-f)\,, \\
\frac{du_{i,j}}{dt} &= \frac{\frac{d^2u_{i,j}}{dx^2}\left(\left(\frac{du_{i,j}}{dy}\right)^2+\epsilon^2\right)-2\left(\frac{du_{i,j}}{dx}\right)\left(\frac{du_{i,j}}{dy}\right)\left(\frac{d^2u_{i,j}}{dxdy}\right)+\frac{d^2u_{i,j}}{dy^2}\left(\left(\frac{du_{i,j}}{dx}\right)^2+\epsilon^2\right)}{\left(\left(\frac{du_{i,j}}{dx}\right)^2+\left(\frac{du_{i,j}}{dy}\right)^2+\epsilon^2\right)^{\frac{3}{2}}} \\
&- \frac{1}{\alpha}\left(u_{i,j}-f_{i,j}\right)
\end{aligned}
\tag{15}
$$

where

$$
\frac{d^2u_{i,j}}{dxdy}\approx\frac{u_{i+1,j+1}-u_{i+1,j-1}-u_{i-1,j+1}+u_{i-1,j-1}}{4}\,. \tag{16}
$$

When explicit time discretization is employed, numerical solution to Equation (15) can be computed by the following iterative scheme, where homogeneous Neumann boundary condition is imposed along the image boundary:

$$
\begin{aligned}
\frac{u_{i,j}^{k+1}-u_{i,j}^k}{\Delta t} &= \left(\left(\frac{u_{i+1,j}^k-u_{i-1,j}^k}{2}\right)^2+\left(\frac{u_{i,j+1}^k-u_{i,j-1}^k}{2}\right)^2+\epsilon^2\right)^{-\frac{3}{2}} \\
&\cdot\Bigg[\left(u_{i+1,j}^k-2u_{i,j}^k+u_{i-1,j}^k\right)\left(\left(\frac{u_{i,j+1}^k-u_{i,j-1}^k}{2}\right)^2+\epsilon^2\right) \\
&- \frac{1}{8}\left(u_{i+1,j}^k-u_{i-1,j}^k\right)\left(u_{i,j+1}^k-u_{i,j-1}^k\right) \\
&\quad\left(u_{i+1,j+1}^k-u_{i+1,j-1}^k-u_{i-1,j+1}^k+u_{i-1,j-1}^k\right) \\
&+ \left(u_{i,j+1}^k-2u_{i,j}^k+u_{i,j-1}^k\right)\left(\left(\frac{u_{i+1,j}^k-u_{i-1,j}^k}{2}\right)^2+\epsilon^2\right)\Bigg] \\
&- \frac{1}{\alpha}\left(u_{i,j}^k-f_{i,j}\right)
\end{aligned}
\tag{17}
$$

where Δt denotes the time step. ϵ-regularization requires the stability condition $\Delta t \leq 0.25\epsilon$, and thus a sufficiently large number of iterations is needed for small values of ϵ.

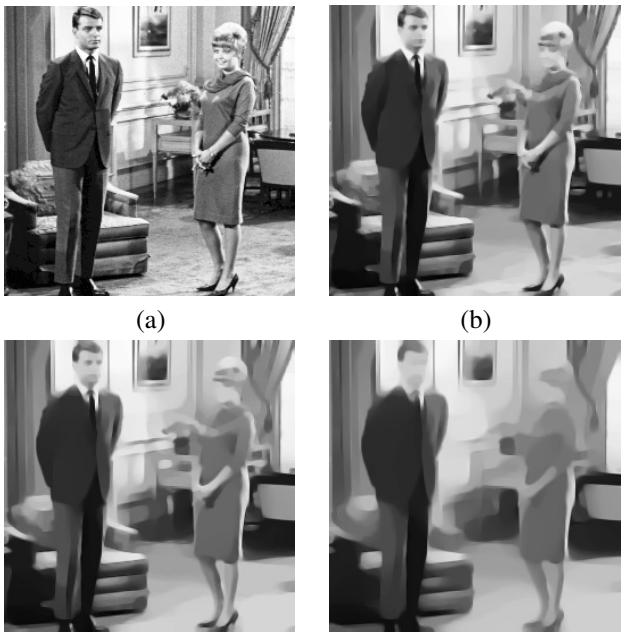

Figure 6: Example TV restoration results. (a) Source image. (b)-(d) Corresponding segmentations obtained with (b) $\alpha = 50$, (c) $\alpha = 100$, and (d) $\alpha = 200$.

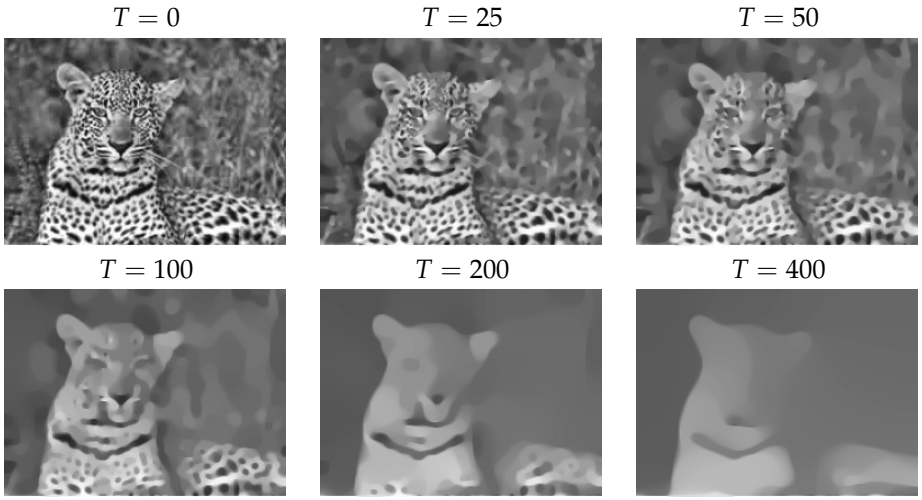

Figure 7: TV flow results for different diffusion times.

3 EDGE ENHANCING DIFFUSION

The nonlinear diffusion model proposed by Perona and Malik employs a scalar-valued diffusivity function to guide the smoothing process as summarized in Section 1. The diffusivities are reduced at the image locations where the magnitude of image gradient $|\nabla u|^2$ is large, and as a result, the edges are preserved or even enhanced. In [6],

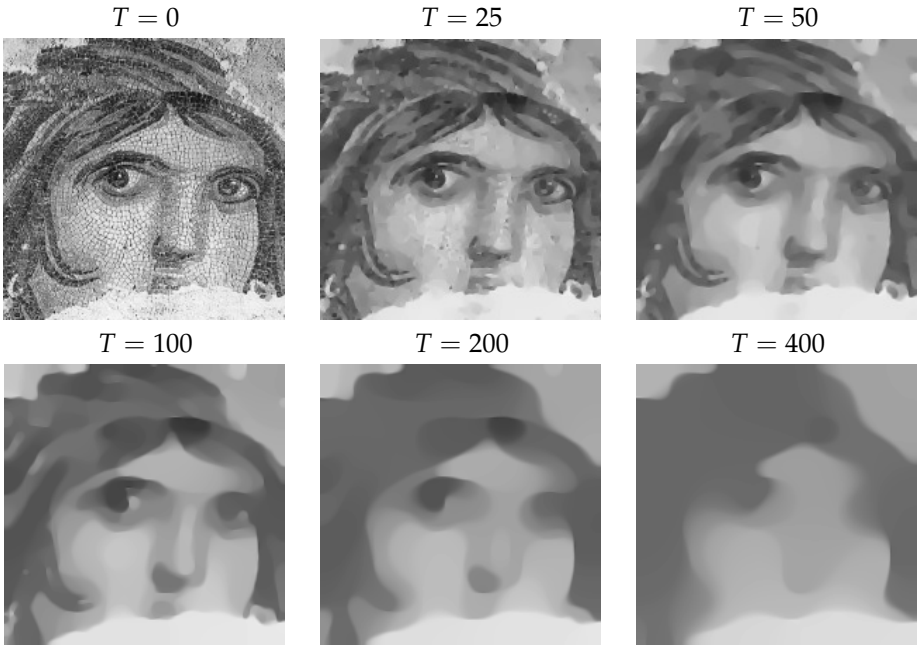

Figure 8: TV flow results for different diffusion times.

Weickert suggested an alternative approach that additionally takes direction of the image gradients into account. The suggested model is an anisotropic nonlinear diffusion model with better edge enhancing capabilities.

In general, any anisotropic nonlinear diffusion can be described by the equation

$$\frac{\partial u}{\partial t} = \nabla \cdot (D(\nabla u)\nabla u) \tag{18}$$

where u is the smoothed image that is initialized with the input image f (that is $u^0(x) = f(x)$), and D represents a matrix-valued diffusion tensor that describes the smoothing directions and the corresponding diffusivities. One can easily observe that for linear diffusion the diffusion tensor can be defined as $D(\nabla u) = I$, which results in a constant diffusion coefficient for all image points in all directions. Similarly, for Perona-Malik type nonlinear diffusion, $D(\nabla u) = g(|\nabla u_\sigma|)I$. Such a choice reduces the amount of smoothing at image edges, but in an equal amount in all directions. In actual anisotropic setting, the diffusion tensor D is defined as a function of the structure tensor given by

$$J(\nabla u) = \nabla u \nabla u^T = \begin{bmatrix} u_x^2 & u_x u_y \\ u_x u_y & u_y^2 \end{bmatrix}. \tag{19}$$

The structure tensor $J(\nabla u)$ can be interpreted as an image feature describing the local orientation information. It has an orthonormal basis of eigenvectors v_1 and v_2 with $v_1 \parallel \nabla u$ and $v_2 \perp \nabla u$, and the corresponding eigenvalues $\lambda_1 = |\nabla u|^2$ and $\lambda_2 = 0$. It is important to note that noise significantly affects the tensor estimation.

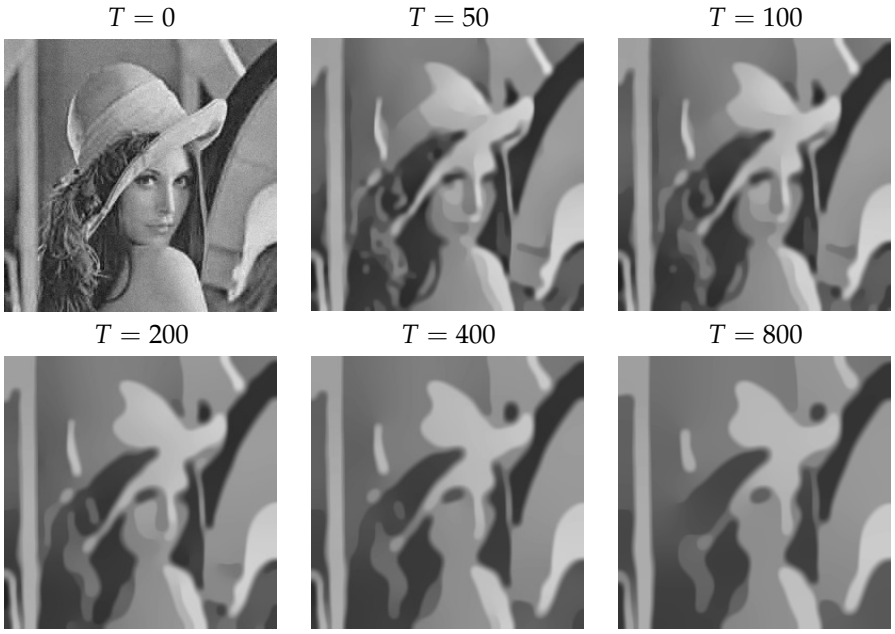

Figure 9: Edge enhancing diffusion results for different diffusion times ($\lambda = 2, \sigma = 1$).

Thus the given image u is usually convolved with a Gaussian kernel G_σ with a relatively small standard deviation σ as a presmoothing step and the structure tensor is computed accordingly by using $\nabla u_\sigma = \nabla(G_\sigma * u)$ instead of ∇u.

The main idea behind edge enhancing diffusion is to use the structure tensor as an image/edge descriptor to construct a diffusion tensor that reduces the amount of smoothing across the edges while smoothing is still carried out along the edges. In order to perform this, Weickert proposed to utilize same orthonormal basis of eigenvectors $v_1 \parallel \nabla u_\sigma$ and $v_2 \perp \nabla u_\sigma$ estimated from the structure tensor $J(\nabla u_\sigma)$ with the following choice of eigenvalues satisfying $\frac{\lambda_1(|\nabla u_\sigma|)}{\lambda_2(|\nabla u_\sigma|)} \to 0$ for $|\nabla u_\sigma| \to \infty$

$$\lambda_1(|\nabla u_\sigma|) = \begin{cases} 1 & \text{if } |\nabla u_\sigma| = 0 \\ 1 - exp\left(-\frac{3.31488}{(|\nabla u_\sigma|/\lambda)^8}\right) & \text{otherwise,} \end{cases} \tag{20}$$

$$\lambda_2(|\nabla u_\sigma|) = 1 \tag{21}$$

where λ denotes the contrast parameter.

Such a choice preserves and enhances image edges by reducing the diffusivity λ_1 perpendicular to edges for sufficiently large values of $|\nabla u_\sigma|$. Specifically, the diffusion tensor is given by the formula

(22)

$$D = \begin{bmatrix} (u_\sigma)_x & -(u_\sigma)_y \\ (u_\sigma)_y & (u_\sigma)_x \end{bmatrix} \cdot \begin{bmatrix} \lambda_1(|\nabla u_\sigma|) & 0 \\ 0 & \lambda_2(|\nabla u_\sigma|) \end{bmatrix} \cdot \begin{bmatrix} (u_\sigma)_x & -(u_\sigma)_y \\ (u_\sigma)_y & (u_\sigma)_x \end{bmatrix}^{-1}.$$

Figure 9 and Figure 10 illustrate example results of edge enhancing diffusion filter

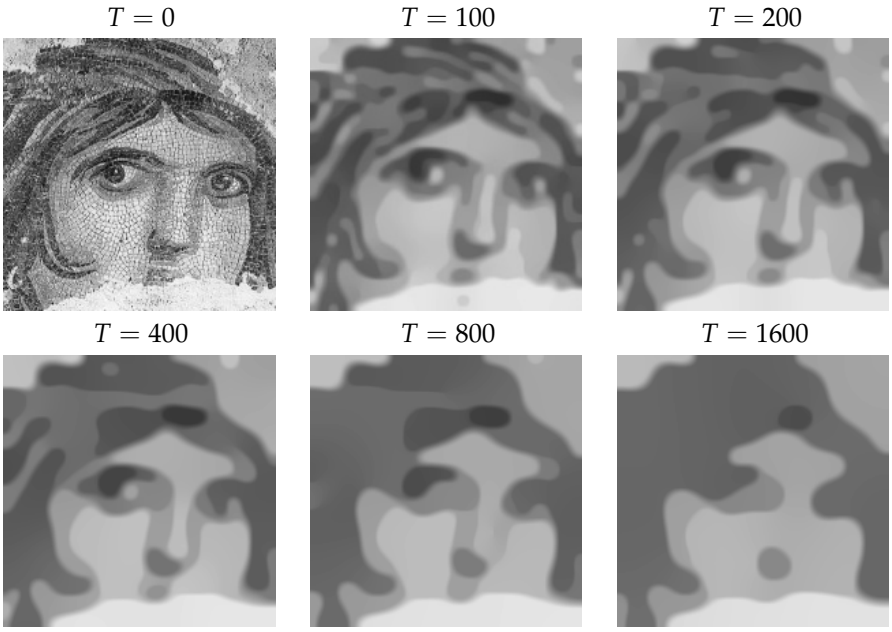

Figure 10: Edge enhancing diffusion results for different diffusion times ($\lambda = 1.8$, $\sigma = 1$).

for different diffusion times. As it can be clearly seen from these images, the corresponding smoothing process diminishes noise and fine image details while retaining and even enhancing edges as in the Perona-Malik type nonlinear diffusion. On the other hand, the corners become more rounded in the anisotropic model compared to the Perona-Malik filter (cf. Figure 3 and Figure 4) since edge enhancing diffusion allows smoothing along edges while preventing smoothing across them. As discussed in [7], this causes a slight shrinking effect in the image structures, which eliminates fine or thin structures better than the Perona-Malik model. Thus, through this process one can capture semantically more correct image regions.

REFERENCES

[1] F. Andreu, C. Ballester, V. Caselles, and J. M. Mazón. Minimizing total variation flow. *Differential and Integral Equations*, 14(3):321–360, 2001.

[2] F. Catté, P.-L. Lions, J.-M. Morel, and T. Coll. Image selective smoothing and edge detection by nonlinear diffusion. *SIAM J. Numer. Anal.*, 29(1):182–193, 1992.

[3] F. Dibos and G. Koepfler. Global total variation minimization. *SIAM J. Numer. Anal.*, 37(2):646–664, 2000.

[4] P. Perona and J. Malik. Scale-space and edge detection using anisotropic diffusion. *IEEE Trans. Pattern Anal. Mach. Intell.*, 12:629–639, 1990.

[5] L. Rudin, S. Osher, and E. Fatemi. Nonlinear total variation based noise removal algorithms. *Phys. D.*, 60:259–268, 1992.

[6] J. Weickert. Anisotropic diffusion filters for image processing based quality control. In *Proc. Seventh European Conference on Mathematics in Industry*, pages 355–362, 1994.

[7] J. Weickert. *Anisotropic Diffusion in Image Processing.* Teubner, Stuttgart, 1998.